Field and experimental evaluation of a probabilistic-based health indicator for efficient road health monitoring via FBG sensor network

Golmohammadi, Ali; Yaghoubi, Vahid; Ghaderi, Nasser; Hasheminejad, Navid; Lajnef, Nizar; Van den bergh, Wim; Hernando, David

DOI
10.1177/14759217251393491

Publication date
2025

Document Version
Final published version

Published in
Structural Health Monitoring

Original Research Article

Structural Health Monitoring
1–15

DOI: 10.1177/14759217251393491
journals.sagepub.com/home/shm
Sage

Field and experimental evaluation of a probabilistic-based health indicator for efficient road health monitoring via FBG sensor network

Ali Golmohammadi[1], Vahid Yaghoubi[2], Nasser Ghaderi[3], Navid Hasheminejad[1], Nizar Lajnef[4], Wim Van den bergh[1] and David Hernando[1]

Abstract

Structural health monitoring (SHM) of infrastructure using sensor networks presents significant challenges, particularly for linear structures that require extensive coverage of critical hotspots. Among the various sensing technologies, optical fiber sensors have recently gained attention as a promising solution for distributed and long-span monitoring due to their ability to provide a high density of sensing points. However, the vast amounts of data generated by these sensors create substantial challenges in data handling, processing, management, and analysis. These challenges are further intensified under random loading and unknown conditions, where discerning patterns becomes particularly difficult. To address these issues, this study proposes a probabilistic-based framework for generating a health indicator (HI) through cumulative loading-time analysis of sensor data. The method reduces data dimensionality by calculating cumulative loading time within predefined windows and strain levels, thereby extracting meaningful features by fitting a cumulative distribution function. These features are then used to construct sensor-specific distributions, and Kullback–Leibler divergence is employed to monitor shifts between a trained baseline distribution and the current distribution. This produces the HI, enabling quantitative tracking of distribution shifts caused by structural changes or long-term anomalies. The proposed approach was validated through experimental fatigue tests, in which strain sensors monitored responses during fatigue progression. Results demonstrated the method's effectiveness in detecting and localizing damage in two scenarios: when damage occurred directly at sensor locations and when it occurred nearby. Furthermore, the method was evaluated using both healthy-state field data and synthetic damage data generated from a fiber Bragg grating sensor network embedded in a roadway. This real-world scenario, characterized by random and unknown-magnitude loading, further validated the method's robustness and applicability. Overall, the results demonstrate the potential of the proposed framework for practical deployment in SHM systems, offering efficient monitoring using large-scale sensor networks.

Keywords

Health indicator, data dimensionality reduction, fiber Bragg grating, optical fiber sensors, cumulative loading-time analysis, road health monitoring

Introduction

Emerging sensor technologies are playing a pivotal role in advancing structural health monitoring (SHM) systems, offering unprecedented capabilities for real-time monitoring of infrastructure such as roads, bridges, buildings, and dams. These sensors, including fiber optic,[1–4] piezoelectric,[5–8] accelerometer,[9–11] acoustic emission,[12–15] ultrasonics,[16,17] sensor networks, among others,[18] enable continuous collection of large datasets that reflect the health and performance of structures over time. In recent years, optical fiber sensors have

[1]SuPAR Research Group, Faculty of Applied Engineering, University of Antwerp, Antwerp, Belgium
[2]Q-VAIbe research group, Department of Aerospace Structures and Material, Faculty of Aerospace Engineering, Delft University of Technology, Delft, The Netherlands
[3]InViLab Research Group, University of Antwerp, Groenenborgerlaan, Antwerp, Belgium
[4]Department of Civil and Environmental Engineering, Michigan State University, East Lansing, MI, USA

Corresponding author:
Ali Golmohammadi, SuPAR Research Group, Faculty of Applied Engineering, University of Antwerp, Antwerp, Belgium.
Email: SeyedAli.GolmohammadiTavalaei@uantwerpen.be

emerged as a promising technology in the field of SHM, owing to their ability to provide either quasi-distributed sensing—through fiber Bragg gratings (FBGs)—or fully distributed sensing using distributed optical fiber technologies. These capabilities enable continuous or point-specific monitoring across large-scale structures with high precision and reliability.[19–22] These sensors also enable the precise measurement of strain, temperature, and other physical parameters with multiplexing capability and immunity to electromagnetic fields.[23–25] Their ability to offer real-time, high-resolution data makes them invaluable for detecting localized issues and potential failures in infrastructure. However, the widespread deployment of optical fiber sensors introduces significant challenges in monitoring, processing, and analyzing these large datasets. In addition to computational demands, integrating such heterogeneous sensor data into existing infrastructure or pavement management systems remains a critical hurdle, as many current systems are not designed to handle the volume, complexity, and variety of SHM data. This underscores the need for standardized data formats, interoperability guidelines, and unified interpretation frameworks to enable seamless data exchange and integration across platforms and regions.[26,27]

The distributed nature of optical fiber sensors leads to complex data sets, necessitating sophisticated algorithms and advanced data management techniques to ensure the effective extraction of meaningful insights.[28] Therefore, efficient data handling methods are essential to prevent information overload and ensure that valuable data can be quickly analyzed for timely decision-making in structural maintenance and repair.

To address these challenges, data reduction techniques can be employed to manage the large volumes of data generated by sensors. Data reduction methods aim to reduce the data size by eliminating unnecessary information while preserving essential features, enabling more efficient processing and analysis. Approaches such as dimensionality reduction help simplify complex datasets by reducing the number of variables, thereby minimizing computational load. This approach contributes to faster processing times and more effective management of sensor data, facilitating real-time analysis and decision-making.

Different studies have proposed and implemented various data reduction approaches for this purpose, such as random projection,[29] robust multidimensional scaling,[30] principal component analysis,[31] and t-distributed stochastic neighbor embedding,[32] among others. Another approach, proposed by several studies,[33–37] is based on cumulative measurement and probabilistic theory. The main advantage of this method is that it relies on relative variations in the response distribution, eliminating the need to measure damage directly. Moreover, since most damage propagation mechanisms—such as fatigue and cracking—occur incrementally with small-scale changes that accumulate over time and exhibit nonlinear progression, this method is particularly beneficial and has been validated for piezoelectric and strain gauge (SG) sensor data.[33–37] The final output of this method is response distributions over time, which can be compared to detect potential damage initiation. However, in a deployed network with numerous sensors, tracking all distributions across the network becomes challenging. To address this issue, this study explores how these distributions can be transformed into a health indicator (HI), a simplified representation that facilitates the simultaneous monitoring of trends and patterns across a large number of sensors. The HI is a key feature in SHM as it reflects the health status of the system or structure and provides actionable insights. Although HIs can be constructed using various methods, they must meet three critical characteristics: detectability,[38] ensuring that damage can be detected; separability,[38] allowing distinction between healthy and damaged states; and trendability,[39] enabling the clear observation of gradual changes over time.[40] The construction of a suitable HI is a critical step before predicting the remaining useful life of a system using a prognostic model.[41,42] Identifying the most effective and optimal HI based on different methods remains a prominent research focus in the field of SHM.

The primary objective of this study is to develop a probabilistic-based framework that adopts Kullback–Leibler (KL) divergence within a cumulative loading time analysis for transforming the large volume of data collected from FBG sensor networks into meaningful and sensitive HIs that reflect changes in structural health. Cumulative loading-time analysis was chosen as it is well suited for real-world conditions where loading is random; KL divergence was selected because it quantifies differences between two probability distributions in a way that is sensitive to shifts in mean values and changes in variability. The HIs are intended to capture variations in sensor data caused by material or structural changes, such as fatigue, occurring either at the sensor location or in its vicinity. This study builds upon our previous work on a different test track that focused on preprocessing and local anomaly detection[43] as a necessary step prior to the development of health indices in this research. Here, the main focus is on the global analysis of SHM data, aiming to identify long-term changes or anomalies that indicate structural deterioration rather than local data analysis. By adapting KL divergence within a cumulative loading-time framework, the proposed methodology produces scalable and efficient HIs, uniquely enabling data compression for large sensor networks and long-term trend

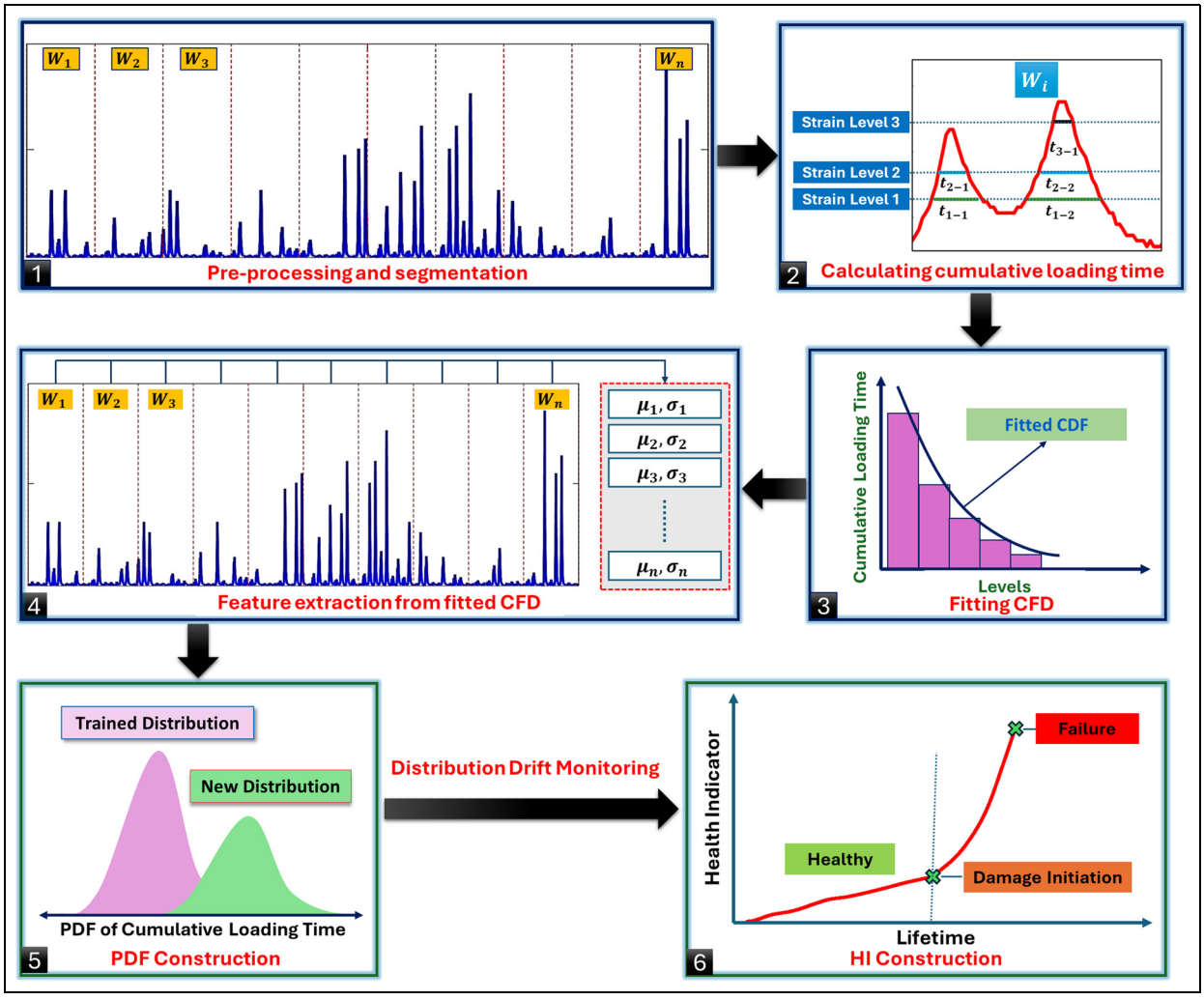

Figure 1. Methodology of constructing HI. HI: health indicator.

detection for structural deterioration. By leveraging these HIs, the framework aims to enable the simultaneous snapshot monitoring of large-scale sensor networks, support real-time detection and assessment of structural damage, and inform timely maintenance decisions, ultimately laying the foundation for a scalable monitoring system for road infrastructure.

Methodology

The overall framework employed in this study is based on cumulative loading-time measurement and probability theory.[33–37] This approach consists of a systematic sequence of six key steps, which are depicted in Figure 1. First, data are collected, preprocessed, and segmented into windows containing the same number of data points (step 1). Next, the cumulative loading time is calculated at predefined levels for each window in a cumulative manner, capturing the strain accumulation over time (step 2). Then, for each window, a cumulative time histogram is constructed, and a cumulative distribution function (CDF) is fitted to the data to represent the distribution of cumulative loading over time. Previous studies have demonstrated that the best CDF for this purpose is the Gaussian function,[33,34] expressed as follows:

$$F_{\text{Gaussian}}(\varepsilon) = \frac{A}{2}\left[1 - erf\left(\frac{\varepsilon - \mu}{\sigma\sqrt{2}}\right)\right] \quad (1)$$

Here, A is the summation of all cumulative time events, and σ and μ are the standard deviation and mean of the CDF, respectively (step 3). Following that, key statistical features μ and σ are extracted from the fitted CDF of each window, capturing changes in the strain distribution that reflect gradual alterations in structural behavior. Since these parameters can fluctuate under variable loading conditions, a median filter is

used to smooth μ and σ, reducing abnormal deviations and minimizing the influence of non-Gaussian noise in the data (step 4). Subsequently, a probability density function (PDF), parameterized by the extracted μ and σ, is constructed for each window, which offers a probabilistic representation of the structural health status and potential long-term anomalies (step 5). A baseline PDF is first constructed from strain data corresponding to the confirmed healthy (or relatively healthy) state of the structure. This baseline should include variations in environmental and loading conditions to serve as a reliable reference for monitoring; this is particularly important with temperature- and loading time-dependent materials, such as asphalt. A certain percentage (i.e., 20%) of the healthy-state data from each sensor is reserved for this purpose, and all subsequent monitoring windows are benchmarked against this baseline. In addition to these steps, this study introduces a novel method based on distribution drift monitoring (DDM) to construct a HI (step 6). Given the challenges of tracking distribution drift over time across multiple sensors, this approach enables the simultaneous comparative monitoring of large sensor networks within a single plot. The constructed HI facilitates the detection of damage and potential long-term anomalies in SHM data from large civil infrastructure. This unified visualization supports efficient and scalable assessment of structural health over time.

There are several methods for data DDM, with one of the most effective being the KL divergence,[44] also known as relative entropy. KL divergence serves as a statistical measure to quantify the dissimilarity between two probability, offering higher sensitivity compared to alternative DDM measures (e.g., Wasserstein distance and Jensen–Shannon divergence). This property makes it particularly useful for the early detection of distribution shifts or variations. The KL divergence between two Gaussian distributions $P \sim \mathcal{N}(\mu_1, \sigma_1^2)$ and $Q \sim \mathcal{N}(\mu_2, \sigma_2^2)$ can be derived from its general definition as follows[44]:

$$D_{\mathrm{KL}}(PQ) = \int_{-\infty}^{\infty} P(x) \log \frac{P(x)}{Q(x)} \mathrm{d}x \tag{2}$$

By substituting the distributions P and Q into Equation (2) and simplifying, the final expression for the KL divergence is obtained as follows[45]:

$$D_{\mathrm{KL}}(P \| Q) = \log \frac{\sigma_2(i)}{\sigma_1} + \frac{\sigma_1^2 + (\mu_1 - \mu_2(i))^2}{2\sigma_2(i)^2} - \frac{1}{2} \tag{3}$$

Here, μ_1 and σ_1 correspond to the trained baseline distribution P, while $\mu_2(i)$ and $\sigma_2(i)$ correspond to the current distribution $Q(i)$. In this study, a portion of the data collected during the healthy state of a structure is used to train a baseline distribution P, representing the undamaged condition. At each subsequent time i, a new distribution $Q(i)$ is fitted to the updated data (next windows). The KL divergence between the trained baseline P and the current distribution $Q(i)$ is then calculated as the HI:

$$\mathrm{HI} = D_{\mathrm{KL}}(P \| Q(i)) \tag{4}$$

In this study, no fixed or adaptive threshold was applied to the HI. Nonetheless, threshold determination for failure detection is considered an important future step.

Experimental measurement and validation

To validate the proposed HI for damage detection and localization, an experimental fatigue test was conducted using the four-point bending test under load-controlled conditions in a climate chamber. This test setup was selected because it enables measuring a fairly uniform strain field in the central area of the sample and allows introduction of temperature variations. In this study, the temperature was intentionally varied in a random manner during testing to simulate in situ environmental conditions more realistically. For this test, three beam samples with dimensions 60 × 60 × 400 mm were fabricated, and foil SGs were installed on the bottom side of the samples within a shallow groove (10 mm wide, 4 mm deep) to prevent interference of sensor wires with the supports (see Figure 2). The sensors were placed in the region between the two internal supports, where the strain distribution is uniform, and the likelihood of damage occurrence is the highest. In the first test, three SGs with a length of 10 mm were used. To cover a larger area, an additional longer SG with a length of 20 mm was incorporated in the subsequent two tests.

Figure 3 illustrates the configuration of the SGs, their numbering, and the location of the cracks after the fatigue tests. The crack in sample 1 occurred outside the region covered by the installed sensors. In sample 2, the crack propagated beneath SG 3, damaging it. For sample 3, the crack initiated directly beneath SG 1.

During the test, strain responses were sampled at 500 Hz using an EDX-10 compact recording system and processed with the DCS-100A software. Figure 4 illustrates the SG responses during the fatigue test for each sample, along with the corresponding temperature variations. As can be seen, some variations in the responses are observed, which can be attributed to random temperature fluctuations imposed during the test. This variability is important for evaluating the

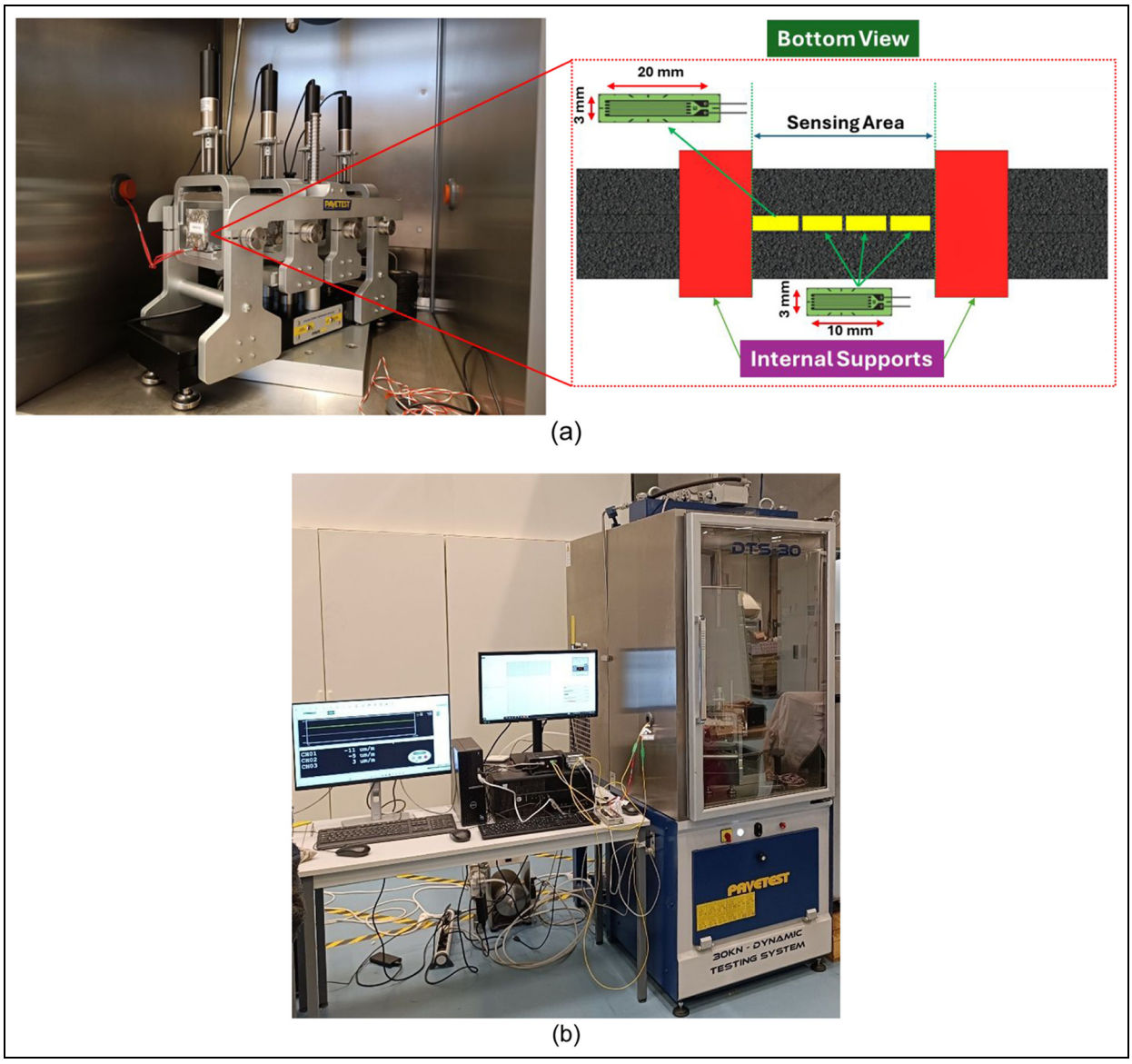

Figure 2. Setup for four-point bending fatigue test: (a) schematic of specimen with installed sensors and (b) dynamic testing system with data acquisition.

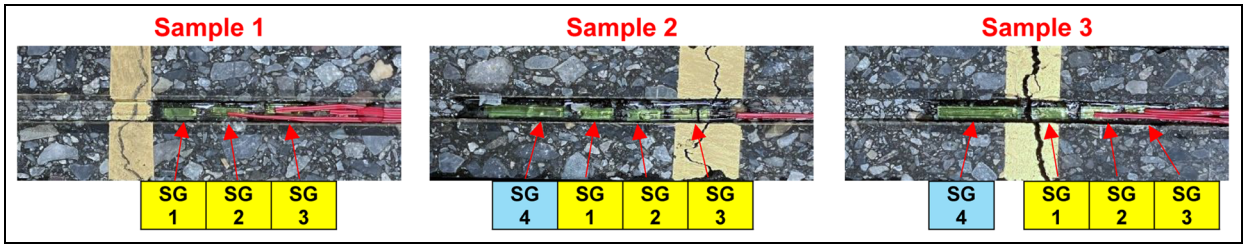

Figure 3. Location of installed SGs along with propagated crack after fatigue tests on three different samples. SG: strain gauge.

robustness of the proposed HI under conditions similar to in situ environments. For sample 1, because of the development of damage cracking outside the sensing area, strain responses from all SGs (SG1, SG2, SG3) exhibit a decreasing trend. In sample 2, crack propagation beneath SG3 led to an increasing strain response

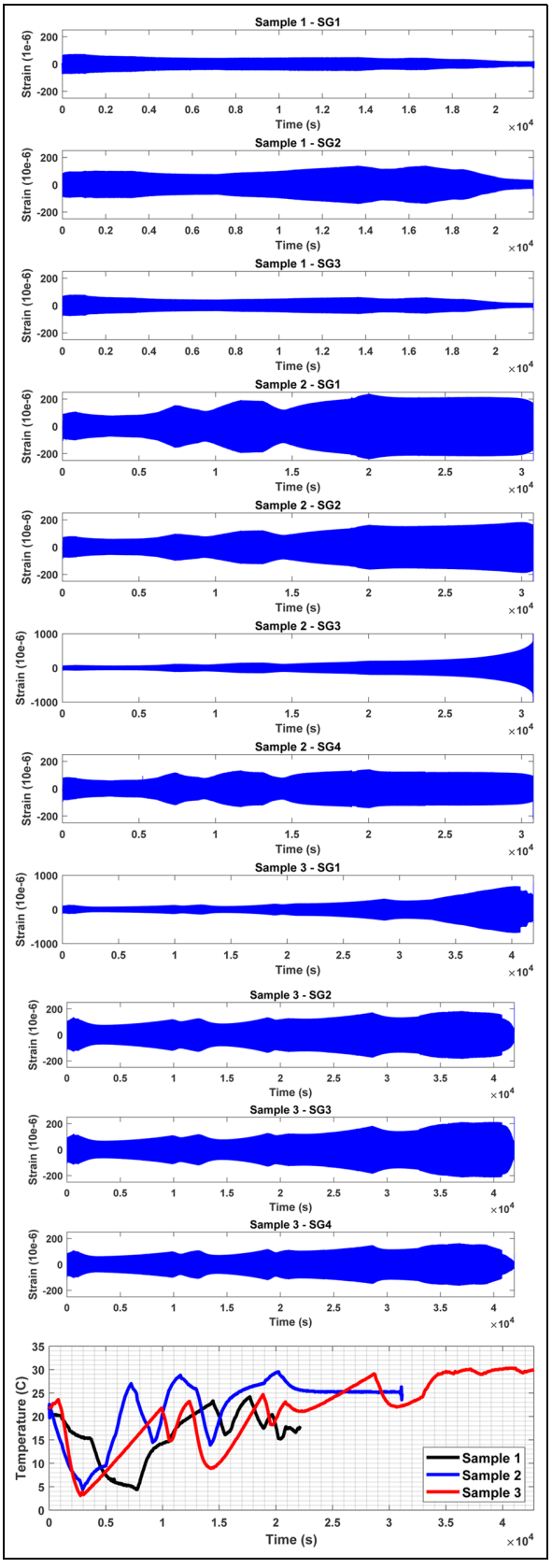

Figure 4. SG responses during fatigue tests and corresponding temperature variations for each sample. SG: strain gauge.

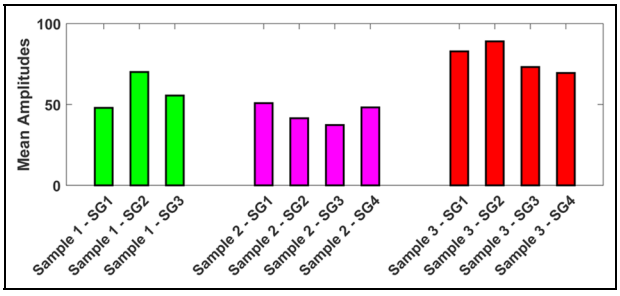

Figure 5. Comparison of mean amplitude of each sensor for all samples (during healthy stage).

in SG3, which eventually rendered the sensor nonfunctional. In contrast, a decreasing strain trend was observed in the other sensors (SG1, SG2, SG4). For sample 3, as the crack initiated beneath sensor 1 (SG1), an increasing strain trend was observed in SG1, while the other sensors (SG2, SG3, SG4) exhibited a decreasing trend.

As a result, these responses demonstrate that an effective HI must be not only sensitive to trends in the data but also capable of identifying damage both at the sensing location and in its vicinity. This is crucial, as damage is more likely to occur in the vicinity of the sensing location rather than directly at it. Therefore, focusing on the vicinity region is critical for accurate damage detection. The experimental laboratory tests were halted when stiffness dropped by 90%, limiting the ability to monitor strain responses further. However, strain levels are expected to remain relatively low compared to historical values. In addition, changes due to environmental effects may be mistaken for damage. However, it is important to note that the impact of environmental factors, such as temperature, on strain responses is typically reversible, whereas strain changes caused by damage are irreversible. This irreversibility in data variation highlights the distinction between environmental effects and damage-induced changes in response. It is also valuable to monitor temperature fluctuations alongside HIs for better accuracy. If the HI and temperature variations follow the same trend, it can be inferred that the structure remains healthy. Conversely, if a deviation between the two trends is observed, damage may be propagating within the structure.

As shown in Figure 4, there is a noticeable difference in the strain response amplitude across all samples. To quantify these differences, the mean amplitude for each sensor was calculated over a short segment at the beginning of the test, when the sample was in a healthy state. The results of this analysis are presented in Figure 5. This observation reflects real-world conditions, where even under the same load and with sensors

installed in the same region, variability in strain response amplitude can still occur due to the inherently heterogeneous nature of asphalt mixtures. Another significant factor contributing to this variability is the bonding quality between the SGs and the specimen. Differences in the adhesive layer's uniformity and bonding strength can lead to variations in strain transfer, even when sensors are located in the same region of the material. As a result, only the trend of variation among the sensors and their relative differences can be meaningfully compared, rather than their absolute values.

Before applying the framework, it is important to note that the robustness and responsiveness of the proposed HI depend on two key parameters: the strain level interval in the cumulative loading-time analysis and the window size used for segmentation. To evaluate their impact, a sensitivity study was conducted on laboratory test data (sample 3, SG1).

The strain level interval controls the resolution at which cumulative strain loading is quantified. Smaller intervals (e.g., 1 or 5 microstrain ($\mu\varepsilon$)) make the HI highly sensitive to short-term and reversible changes, such as fluctuations caused by environmental variations or loading randomness. However, this comes at the cost of increased computational effort and a higher risk of misinterpreting temporary or non-damage-related fluctuations as structural deterioration. Larger intervals (e.g., 15 or 20 $\mu\varepsilon$) reduce sensitivity but increase robustness and computational efficiency, as small-scale fluctuations are smoothed out. As shown in Figure 6(a), increasing the strain level interval progressively reduces the short-term sensitivity of the HI, while making the trend more stable and representative of long-term changes. Based on this trade-off, an interval of 10 $\mu\varepsilon$ was selected in this study, providing a balance between sensitivity to structural deterioration and robustness against environmental variability.

The window size determines the number of datapoints in each segment used to construct cumulative histograms. Smaller windows (e.g., 500 datapoints) provide higher temporal resolution, since the HI is updated more frequently, allowing faster detection of changes. However, the use of smaller windows requires processing a larger number of segments to cover the same monitoring duration, which increases computational demand. In contrast, larger windows (e.g., 6000 datapoints) update the HI less frequently, which improves statistical stability and computational efficiency but delays damage detection. As shown in Figure 6(b), all tested window sizes (500, 1000, 2000, 4000, and 6000) successfully captured the same damage event. However, because the total signal length is fixed, the number of windows varies with the chosen window size. This difference in segmentation explains why the

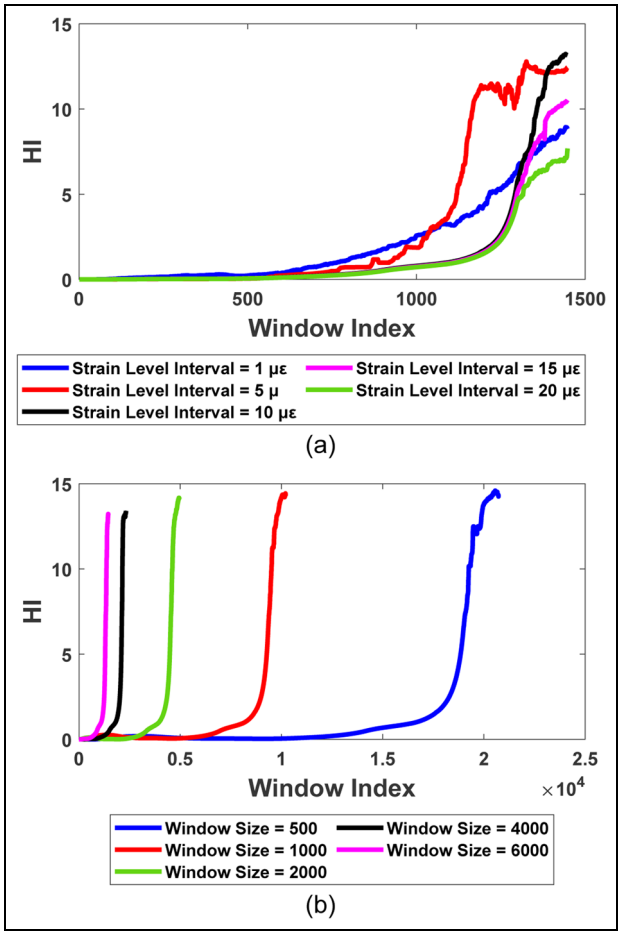

Figure 6. Sensitivity analysis of the HI for sample 3, SG1: (a) effect of strain level interval and (b) effect of window size. HI: health indicator; SG: strain gauge.

detection point appears at different window indices, even though the underlying damage event is the same. Notably, the HI remained stable across all cases, with no excessive fluctuations even at small window sizes, confirming the robustness of the cumulative histogram approach. Based on this analysis, a window size of 2000 datapoints was selected, as it offered a good balance between early sensitivity, computational efficiency, and statistical robustness.

Figure 7 illustrates the HI generated for each sample and SG sensor. For each signal, 20% of the segments were used to establish trained baseline distributions (at healthy status). As shown in Figure 3, cracks occurred beneath SG3 in sample 2 and beneath SG1 in sample 3. A rapid and significant increase in HI can be observed in Figure 7. This highlights the robustness and sensitivity of the proposed HI methodology in detecting and localizing damage. Importantly, the approach eliminates the need for long-term storage of raw data.

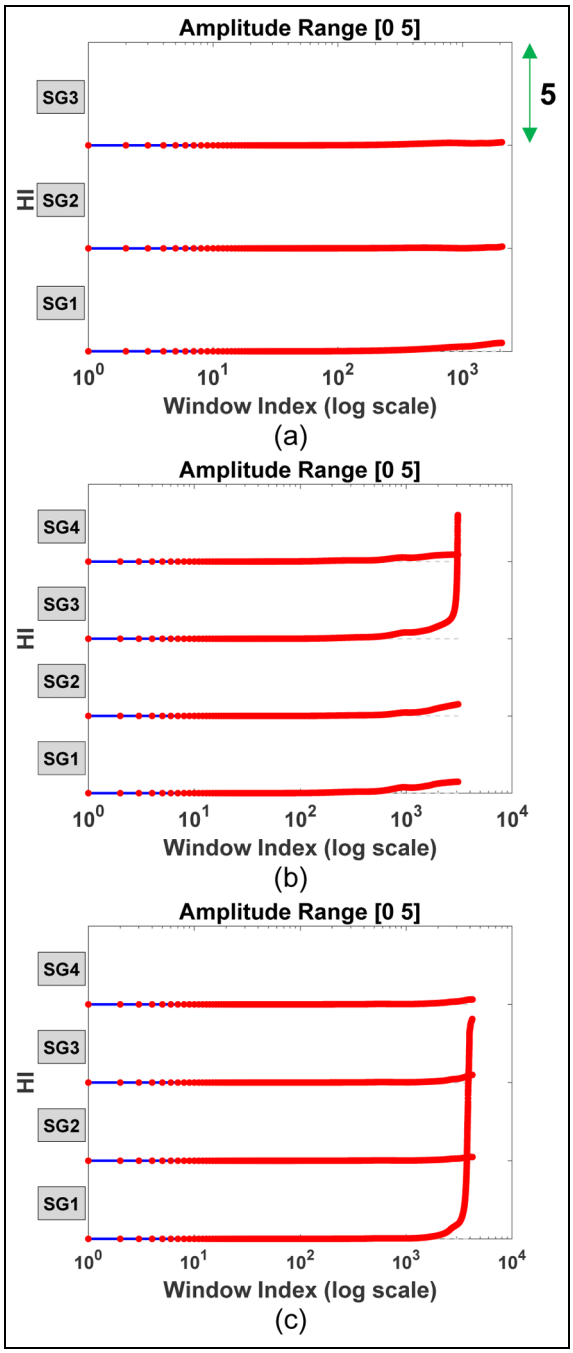

Figure 7. HIs for each sensor installed on samples: (a) sample 1, (b) sample 2, and (c) sample 3. HI: health indicator.

For all sensors in sample 1, as well as the sensors near the crack in samples 2 and 3, a minor increase in HI can be observed. However, if the test had been continued, HI would likely have shown a steeper increase. This conclusion is supported by Equation (3), considering that both the mean and standard deviation of the distribution are expected to decrease under such conditions. Another important consideration is that changes in strain levels occur more slowly when the sensor is located far from the crack compared to when it is placed close to the crack. This is because the strain field dissipates with distance from the crack, leading to a delayed response in detecting cracks initiated near the sensor. Consequently, cracks forming far from the sensor may take longer to be detected. Furthermore, the accuracy and sensitivity of detection are influenced by the distance between the crack and the sensor.

Application to field data

In this phase, the system was evaluated using healthy-state field data and synthetic damage data generated from those measurements collected from one of the three test tracks constructed at the Port of Antwerp-Bruges. More details about the three test tracks can be found in the study by Hernando et al.[46] The test track consisted of two sections (1 and 2) with different asphalt mixtures, each further divided into four subsections (A, B, C, D) at different depths or positions within the lane. In each subsection, a network of FBG sensors was installed according to the configuration illustrated in Figure 8.

As shown in Figure 8, each subsection contains a fiber network with 32 FBG sensors positioned in both transverse and longitudinal directions to monitor the strain and temperature of each layer. Unfortunately, some FBG sensors in each subsection became nonfunctional due to damage sustained during the construction of the test track. The list of operational FBG sensors is provided in Table 1. Strain data from the test track were collected using an eight-channel, 2000 Hz FBG-Scan 708D optical interrogator (FBGS Technologies GmbH, Jena, Germany) connected to the FBG fibers, with a sampling frequency of 100 Hz. The ILLumiSense v2.3.5.5 software (FBGS Technologies GmbH, Jena, Germany) was utilized to convert wavelength shifts into strain and temperature data. To enable continuous monitoring, solar panels and a wind turbine were installed to provide a sustainable power source. The collected data were continuously transmitted to an on-site industrial computer, where they were compressed to about 2% of the original volume. The compressed files were then transferred to a data center equipped with a network-attached storage system and decompressed for offline analysis. This workflow is time-consuming and requires both substantial storage and bandwidth, posing a significant challenge for large-scale monitoring with sensor networks. These constraints highlight the importance of developing frameworks, such as the proposed HI, that can compress SHM data efficiently while still preserving the essential information needed for structural assessment.

After the installation of all equipment, a continuous monitoring campaign was launched, running from

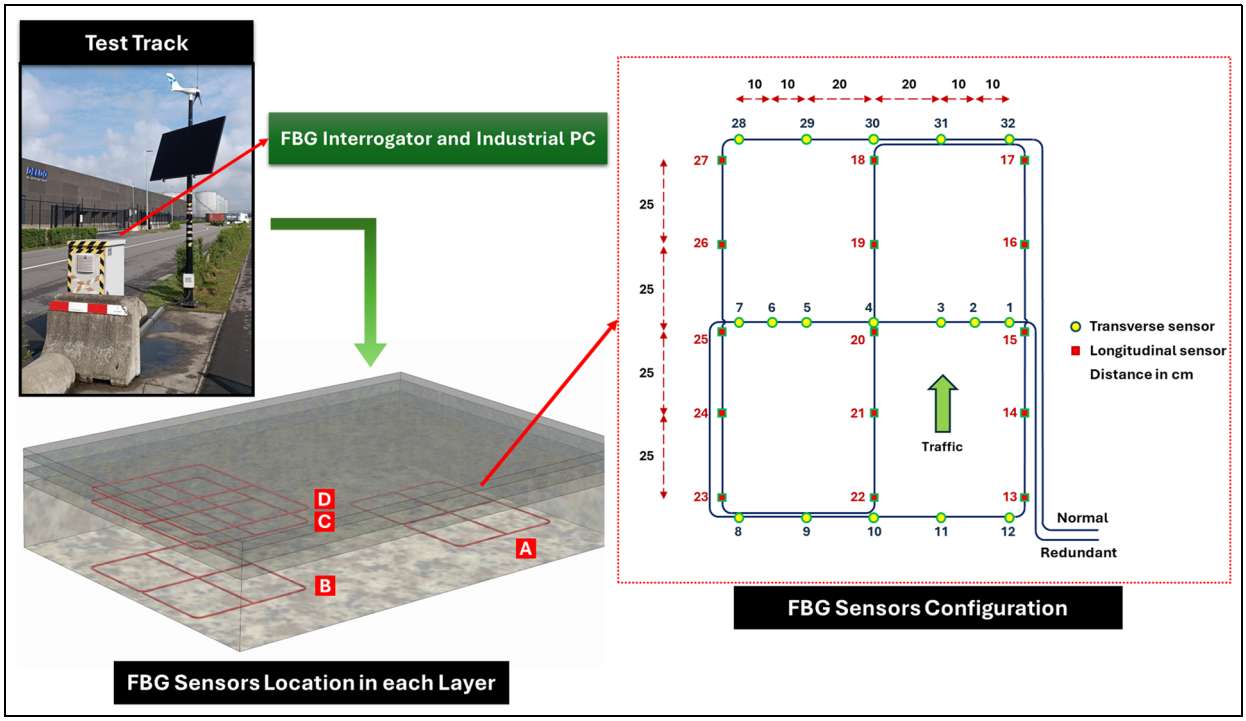

Figure 8. Monitoring test track for pavement monitoring using FBG sensor network. FBG: fiber Bragg grating.

Table 1. List of operational FBG sensors after deployment.

Section	Subsection	Operational FBG sensors
1	A	1–17
1	B	All
1	C	1–7, 28–32
1	D	All
2	A	1–7, 27–32
2	B	20–32
2	C	27–32
2	D	All

FBG: fiber Bragg grating.

Table 2. List of fused FBG sensors group.

Fused group	FBG sensors in group
F1	FBG1, FBG2, FBG3, FBG4, FBG5, FBG6, FBG7
F2	FBG8, FBG9, FBG10, FBG11, FBG12
F3	FBG28, FBG29, FBG30, FBG31, FBG32
F4	FBG13, FBG22, FBG23
F5	FBG14, FBG21, FBG24
F6	FBG15, FBG20, FBG25
F7	FBG16, FBG19, FBG26
F8	FBG17, FBG18, FBG27

FBG: fiber Bragg grating.

April 28, 2024, to October 17, 2024, with a sampling frequency of 100 Hz. Based on prior continuous monitoring conducted on a simpler test track, an FBG sensor network-based monitoring system was developed. This system automates daily data management and preprocessing, incorporating advanced signal processing techniques augmented by a multi-sensor data fusion approach to minimize data variability at each time step i, as expressed by the following equation[43]:

$$F_{\text{data}}(i) = \text{FBG}_j(i) \text{ where } \underset{1 \leqslant j \leqslant p}{j = \text{argmax}} \left| \text{FBG}_j(i) \right| \quad (5)$$

Here, p is the number of FBG sensors that are fused. Prior to fusion, each strain signal was preprocessed to remove temperature-induced strain using wavelet decomposition, as described in our previous study.[43] This process separates the low-frequency (thermal) and high-frequency (traffic load-induced) components, retaining only the latter for subsequent HI computation. In the current study, this process was implemented on a more complex test track, supported by the HI developed as part of this research. The fused sensors are listed in Table 2, where it is noted that all FBG sensors in the same lateral direction were fused as summarized in Table 2. A flowchart of the system is provided in Figure 9. The system's final output consists of HIs for each section, which are further consolidated for each subsection.

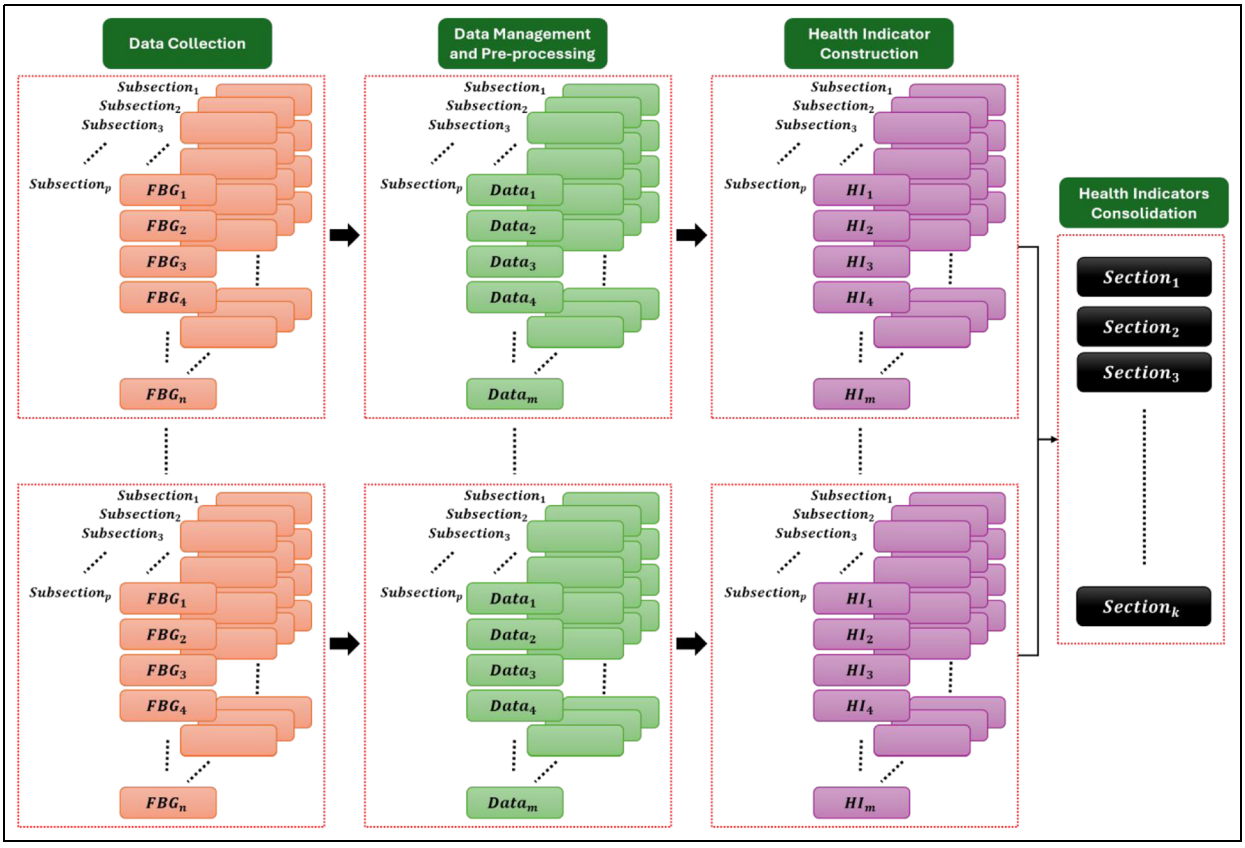

Figure 9. General architecture of the probabilistic-based monitoring system using an FBG sensor network, where p is the number of subsections, n is the number of FBG sensors in each subsection, m is the number of datasets after preprocessing and fusion, and k is the number of sections. FBG: fiber Bragg grating.

Since the HI magnitude is influenced by the proximity of the sensor to the damaged area, the proposed multi-sensor fusion step mitigates this limitation by combining measurements from sensors within the same lateral direction, ensuring that the closest affected sensors contribute most strongly to the HI.

In this study, only positive (tension) traffic load-induced strain was considered. Figure 10 illustrates the HI generated for each subsection based on data from the operational sensors. Similarly, 20% of each FBG data was used for training to construct a trained baseline PDF, representing the healthy state as newly constructed pavement, while the variations in HI shown in Figure 10 correspond to the remaining 80% of the FBG data.

As shown in Figure 10, the data from the network can be efficiently tracked collectively. Depending on the number of datapoints collected, the number of windows varies, which consequently affects the length of the HI. For each subsection, it is clear which datasets exhibit the most significant variations relative to the training data and which ones remain smooth, displaying only minor fluctuations.

Overall, the data indicate that despite some fluctuations, no irrecoverable or significant changes are present, suggesting that the pavement remains in good condition. The observed variations are primarily attributed to external factors, such as environmental effects and loading conditions, which influence changes in the HIs during the monitoring campaign. Notably, certain prominent peaks in the HI data warrant further discussion. For instance, peaks are observed in F1–D of section 2. Detailed analysis revealed that these long-term anomalies correspond to instances when a vehicle was parked over the sensors, as evidenced by distinct patterns in the data shown in Figure 11. Additionally, significant changes in strain levels, likely caused by increased loading or temperature, may also contribute to these peaks over time. This is further illustrated in Figure 11. It is important to note that although thermal strain was removed during preprocessing, traffic load-induced strain remains indirectly influenced by temperature because the asphalt mixtures are temperature-dependent. Consequently, variations in temperature can alter strain levels and, depending on their intensity, affect the HI trend.

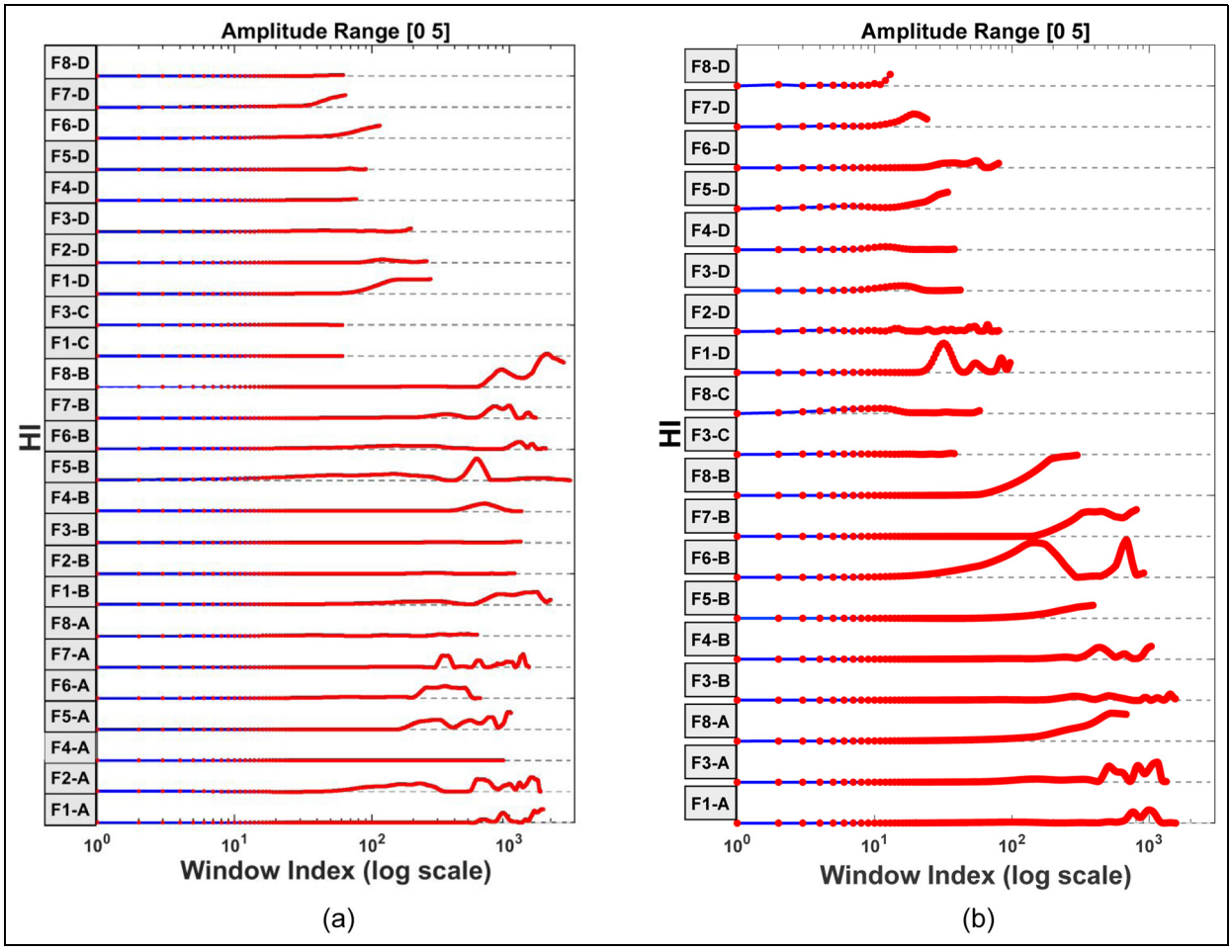

Figure 10. HIs for each section: (a) section 1 and (b) section 2 (F*i*–*j*, where *i* represents the fused group number and *j* denotes the subsection label). HI: health indicator.

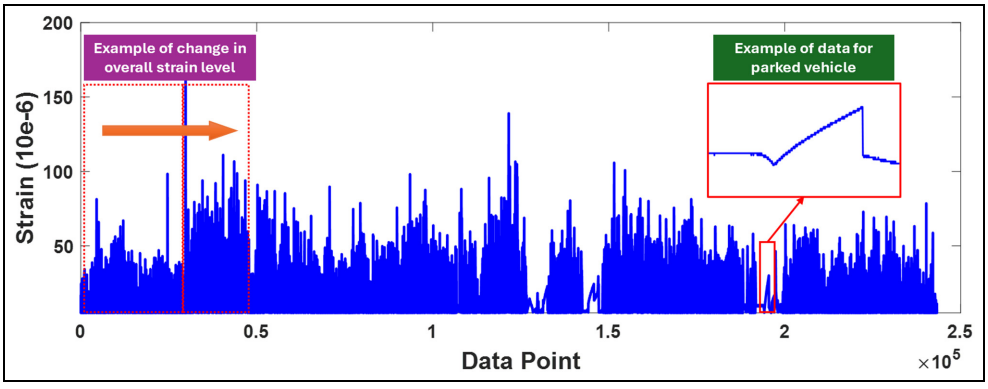

Figure 11. FBG data recorded from F1–D of section 2 that shows the parked vehicles' parent and overall strain level change. FBG: fiber Bragg grating.

These findings underscore the inherent randomness of field data, which is influenced by various parameters that impact HIs. Understanding these potential external influences is essential for interpreting the observed trends.

To confirm that the developed HI can effectively detect damage even in real-world random conditions, one dataset from section 1 (F3–B) was randomly selected to generate synthetic damage data. In the first scenario (see Figure 12(a)), it was assumed that

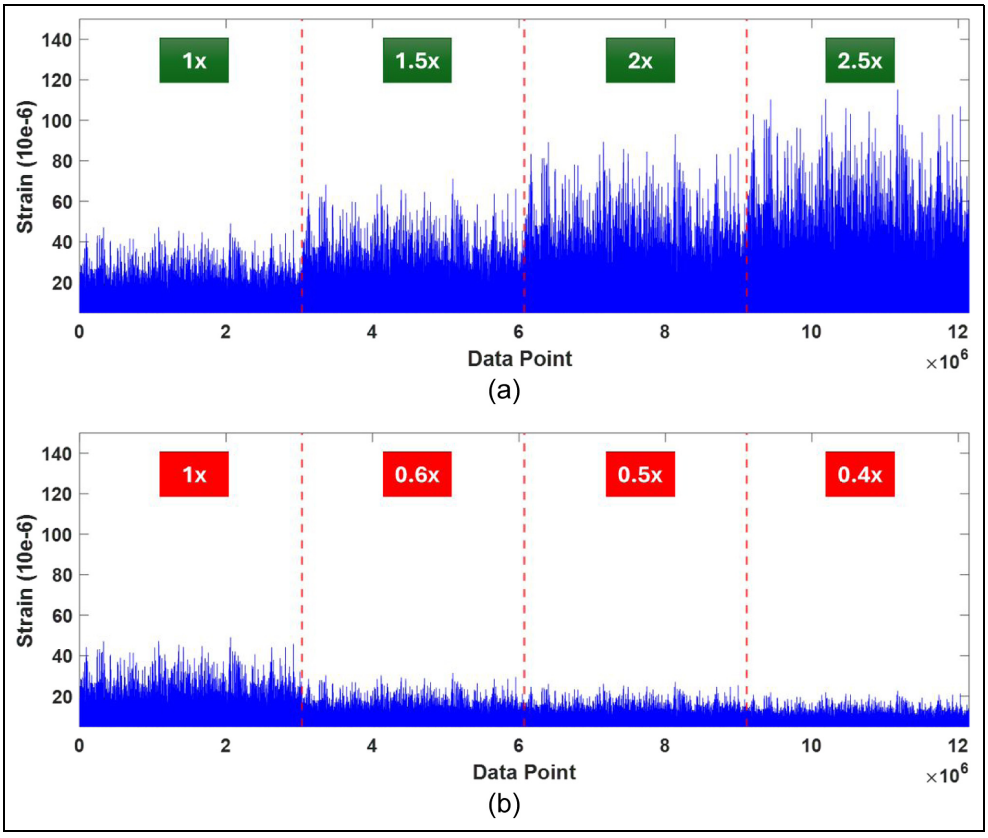

Figure 12. Generated synthetic FBG data for section 1—F3–B to accomplish this objective: (a) scenario 1: synthetic damage at the sensor location and (b) scenario 2: synthetic damage in the vicinity of the sensor. FBG: fiber Bragg grating.

damage propagated at the sensor location, resulting in an increase in the overall strain levels recorded by the sensor over time. For this scenario, the initial recorded signal was amplified by factors of 1.5, 2, and 2.5. In the second scenario (see Figure 12(b)), introduced for greater robustness, it was assumed that damage propagated in the vicinity of the sensor location, leading to a decrease in the overall strain levels recorded by the sensor. In this case, the signal was scaled down by factors of 0.6, 0.5, and 0.4.

The proposed methodology was applied to the synthetic damage data to generate HIs for both scenarios. Figure 13 demonstrates the evolutionary trend of HIs, reflecting significant variations in strain data. In scenario 1, where strain levels increase due to simulated damage propagation at the sensor location, HI exhibits a consistent upward trend. Similarly, in scenario 2, where strain levels decrease due to damage propagation near the sensor, HI also follows an increasing trend, highlighting its ability to capture both strain amplification and reduction effects associated with damage progression.

This study further suggests that defining a fixed or universal threshold for HIs to detect damage is not feasible due to the inherently random and variable nature of field data. Instead, a more robust and reliable approach involves fitting a curve to the HIs over time to capture their underlying evolutionary trends. By analyzing the rate of change of HIs and identifying significant deviations from the baseline trend, it becomes possible to detect early signs of damage. This method leverages the temporal dynamics of HIs, providing a data-driven way to account for randomness while improving the sensitivity and reliability of damage detection.

Conclusions

This study introduces a probabilistic-based framework for constructing HI using FBG sensor networks for road infrastructure health monitoring. By leveraging cumulative loading-time analysis, probability theory, and KL divergence, the proposed approach effectively transforms large-scale sensor data into meaningful indicators capable of detecting and localizing structural damage. The key findings of this study are as follows:

1. Experimental results from four-point bending fatigue tests revealed that damage propagation in

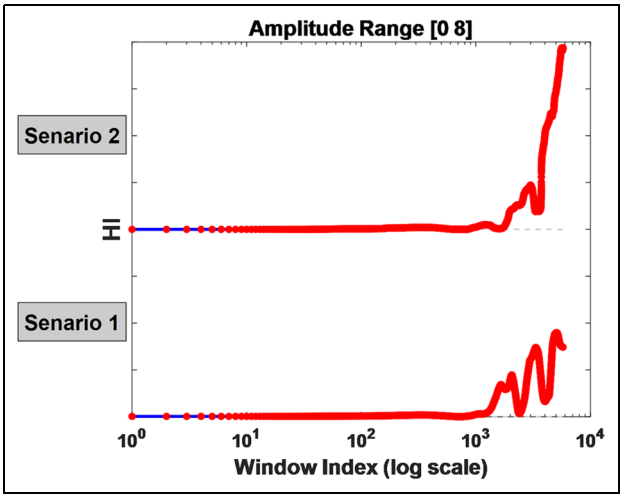

Figure 13. Constructed HI: scenario 1—synthetic damage at the sensor location; scenario 2—synthetic damage in the vicinity of the sensor. HI: health indicator.

materials affected the response of sensors both at the damage location and in its vicinity. The severity of this effect depended on the distance between the damage and the sensor, emphasizing the need for an HI sensitive to both direct and nearby damage.

2. Due to factors such as material heterogeneity, bonding conditions, and aggregate distribution, sensors placed in regions of uniform strain exhibited differing strain responses, underscoring the importance of analyzing relative trends rather than absolute values.
3. Sensitivity analysis showed that smaller strain level intervals and windows detected changes faster but were more variable, while larger ones were more stable but slower. Choosing the right parameters helps balance early detection with reliable long-term monitoring.
4. The methodology was successfully implemented on field data from an FBG sensor network in a long-term monitoring campaign. This demonstrated its feasibility for real-world deployment, even in complex and stochastic field environments.
5. Both experimental and synthetic damage data generated from healthy-state field data analyses indicated that HIs are influenced by damage as well as environmental effects and operational long-term anomalies, such as parked vehicles and loading conditions. Interpreting HIs in the presence of these factors is necessary, as such variability reflects the stochastic nature of real-world applications.

Because of the significant data reduction achieved by converting raw data into a line-type HI, the proposed methodology has the potential to become a scalable and efficient framework for monitoring large sensor networks. By adapting KL divergence within a cumulative loading-time framework, the proposed approach uniquely enables data compression while capturing long-term deterioration trends, both of which are critical for road infrastructure applications. Moreover, while demonstrated here using both FBG and SG sensors, the framework is general and could be extended to other sensing technologies (e.g., piezoelectric sensors). Future research should focus on refining the HI framework, integrating advanced machine learning techniques, and adapting the methodology to other sensor types and infrastructures.

Acknowledgments

The authors thank Com&Sens for their valuable technical support during the sensor installation and data collection phases.

Declaration of conflicting interests

The authors declared no potential conflicts of interest with respect to the research, authorship, and/or publication of this article.

Funding

The authors disclosed receipt of the following financial support for the research, authorship, and/or publication of this article: This study was funded by the Port of Antwerp-Bruges under project 48231, "Durable Pavements for Port Area – Heavily Loaded Pavements: Exploration and In-depth Study." Additionally, the authors gratefully acknowledge the support of the Research Foundation – Flanders (FWO) for funding the research stay that contributed to this work (Grant number: V463524N).

ORCID iDs

Ali Golmohammadi https://orcid.org/0000-0002-8144-2198
Vahid Yaghoubi https://orcid.org/0000-0003-3306-1371

References

1. Yan M, Tan X, Mahjoubi S, et al. Strain transfer effect on measurements with distributed fiber optic sensors. *Autom Constr* 2022; 139: 104262.
2. Li S and Wu Z. Development of distributed long-gage fiber optic sensing system for structural health monitoring. *Struct Health Monit* 2007; 6(2): 133–143.
3. Sigurdardottir DH and Glisic B. On-site validation of fiber-optic methods for structural health monitoring: Streicker Bridge. *J Civ Struct Health Monit* 2015; 5: 529–549.

4. Villalba S and Casas JR. Application of optical fiber distributed sensing to health monitoring of concrete structures. *Mech Syst Signal Process* 2013; 39(1–2): 441–451.
5. Gomasa R, Talakokula V, Jyosyula SKR, et al. A review on health monitoring of concrete structures using embedded piezoelectric sensor. *Constr Build Mater* 2023; 405: 133179.
6. Daraji AH, Ye J and Hale JM. Optimisation of active SHM system based on optimal number and placement of piezoelectric transducers. *J Intell Mater Syst Struct* 2023; 34(4): 425–439.
7. Wong VK, Liu M, Goh WP, et al. Structural health monitoring of fastener hole using ring-design direct-write piezoelectric ultrasonic transducer. *Struct Health Monit* 2022; 21(6): 2657–2669.
8. Zhu C, Xu Z, Hou C, et al. Flexible, monolithic piezoelectric sensors for large-area structural impact monitoring via MUSIC-assisted machine learning. *Struct Health Monit* 2024; 23(1): 121–136.
9. Zhang D, Zhao T, Wang B, et al. Structural health monitoring on operating offshore wind turbine blade via a single accelerometer: feasibility study by simulation and experiment. *Measurement* 2025; 244: 116432.
10. Li XY, Guan YH, Law SS, et al. Monitoring abnormal vibration and structural health conditions of an in-service structure from its SHM data. *J Sound Vib* 2022; 537: 117185.
11. Khan SM, Hanif MU, Khan A, et al. Damage assessment of reinforced concrete beams using cost-effective MEMS accelerometers. *Structures* 2022; 41: 602–618.
12. Lindley CA, Jones MR, Rogers TJ, et al. A probabilistic approach for acoustic emission based monitoring techniques: with application to structural health monitoring. *Mech Syst Signal Process* 2024; 208: 110958.
13. He Y, Li M, Meng Z, et al. An overview of acoustic emission inspection and monitoring technology in the key components of renewable energy systems. *Mech Syst Signal Process* 2021; 148: 107146.
14. Li W, Guo S, Liu Y, et al. Structure health monitoring of composites joint reinforced by acoustic emission based smart composite fasteners. *Composites Commun* 2022; 33: 101213.
15. Sikdar S, Liu D and Kundu A. Acoustic emission data based deep learning approach for classification and detection of damage-sources in a composite panel. *Compos B Eng* 2022; 228: 109450.
16. El Mountassir M, Yaacoubi S, Mourot G, et al. An adaptive PCA-based method for more reliable ultrasonic guided waves SHM: data-driven modeling and experimental validation in high attenuating medium. *Struct Control Health Monit* 2021; 28(1): e2634.
17. Patil S, Banerjee S and Tallur S. Smart structural health monitoring (SHM) system for on-board localization of defects in pipes using torsional ultrasonic guided waves. *Sci Rep* 2024; 14(1): 24455.
18. Hassani S and Dackermann U. A systematic review of advanced sensor technologies for non-destructive testing and structural health monitoring. *Sensors* 2023; 23(4): 2204.
19. Jayawickrema UMN, Herath H, Hettiarachchi NK, et al. Fibre-optic sensor and deep learning-based structural health monitoring systems for civil structures: a review. *Measurement* 2022; 199: 111543.
20. Golmohammadi A, Hasheminejad N and Hernando D. An innovative data analysis approach via peak-counting–based segmentation for pavement monitoring using FBG sensors. *J Test Eval* 2025; 53(2): 271–282.
21. Golmohammadi A, Hernando D, Hasheminejad N, et al. Effect of lateral position and driving conditions on strain pulses recorded by FBG sensors in asphalt pavements. In: *14th international conference on asphalt pavements ISAP2024, Montreal, Canada, 24 December*, 2024, pp. 831–836. Cham: Springer Nature Switzerland AG.
22. Golmohammadi A, Hernando D, Van den Bergh W, et al. Enhanced structural assessment of asphalt pavements using fiber Bragg grating sensors. In: *14th international conference on asphalt pavements ISAP2024, Montreal, Canada, 24 December*, 2024, pp. 59–65. Cham: Springer Nature Switzerland AG.
23. Leung CKY, Wan KT, Inaudi D, et al. Optical fiber sensors for civil engineering applications. *Mater Struct* 2015; 48: 871–906.
24. Sliti M and Boudriga N. Structural health monitoring of road infrastructures based on FBG sensor network. In: *2022 27th Asia Pacific conference on communications (APCC)*, Jeju Island, Republic of Korea, 9–21 October 2022, pp. 36–41. New York: IEEE.
25. Sliti M and Boudriga N.Bridge structural health monitoring using an FBG-based architecture. In: *2021 IEEE International Midwest symposium on circuits and systems (MWSCAS)*, Lansing, MI, USA, 9–11 August 2021, pp. 621–625. New York: IEEE.
26. Abejide S, Mostafa MMH, Das D, et al. Pavement quality index rating strategy using fracture energy analysis for implementing smart road infrastructure. *Sensors* 2021; 21(12): 4231.
27. Hossein AKM, Golroo A and Akhoundzadeh M. Smart embedded technologies and materials for enhanced pavement management. *Autom Constr* 2024; 168: 105865.
28. Mohapatra AG, Talukdar J, Mishra TC, et al. Fiber Bragg grating sensors driven structural health monitoring by using multimedia-enabled IoT and big data technology. *Multimed Tools Appl* 2022; 81(24): 34573–34593.
29. Khoa NLD, Zhang B, Wang Y, et al. Robust dimensionality reduction and damage detection approaches in structural health monitoring. *Struct Health Monit* 2014; 13(4): 406–417.
30. Entezami A, Sarmadi H, Salar M, et al. A novel data-driven method for structural health monitoring under ambient vibration and high-dimensional features by robust multidimensional scaling. *Struct Health Monit* 2021; 20(5): 2758–2777.
31. Kumar K, Biswas PK and Dhang N. Time series-based SHM using PCA with application to ASCE benchmark structure. *J Civ Struct Health Monit* 2020; 10(5): 899–911.
32. Laha SK, Swarnakar B and Kansabanik S. Anomaly detection in structural health monitoring using spectral

distance and t-SNE–GMM framework under ambient excitation. *Asian J Civ Eng* 2024; 25(4): 3711–3727.
33. Bolandi H, Lajnef N, Jiao P, et al. A novel data reduction approach for structural health monitoring systems. *Sensors* 2019; 19(22): 4823.
34. Li X, Bolandi H, Masmoudi M, et al. Mechanics-informed autoencoder enables automated detection and localization of unforeseen structural damage. *Nat Commun* 2024; 15(1): 9229.
35. Manosalvas-Paredes M, Lajnef N, Chatti K, et al. Data compression approach for long-term monitoring of pavement structures. *Infrastructures (Basel)* 2019; 5(1): 1.
36. Alavi AH, Hasni H, Lajnef N, et al. Continuous health monitoring of pavement systems using smart sensing technology. *Constr Build Mater* 2016; 114: 719–736.
37. Hasni H, Alavi AH, Chatti K, et al. A self-powered surface sensing approach for detection of bottom-up cracking in asphalt concrete pavements: theoretical/numerical modeling. *Constr Build Mater* 2017; 144: 728–746.
38. Dempsey P and Brandon EB. Validation of helicopter gear condition indicators using seeded fault tests. In: *59th International instrumentation symposium (IIS)*. Cleveland, Ohio, USA, 1 April 2013. Cleveland, Ohio: NASA Glenn Research Center.
39. Yang F, Habibullah MS, Zhang T, et al. Health index-based prognostics for remaining useful life predictions in electrical machines. *IEEE Trans Ind Electron* 2016; 63(4): 2633–2644.
40. Zhou H, Huang X, Wen G, et al. Construction of health indicators for condition monitoring of rotating machinery: a review of the research. *Expert Syst Appl* 2022; 203: 117297.
41. Moradi M, Gul FC and Zarouchas D. A novel machine learning model to design historical-independent health indicators for composite structures. *Compos B Eng* 2024; 275: 111328.
42. Moradi M, Broer A, Chiachío J, et al. Intelligent health indicator construction for prognostics of composite structures utilizing a semi-supervised deep neural network and SHM data. *Eng Appl Artif Intell* 2023; 117: 105502.
43. Golmohammadi A, Hernando D and Hasheminejad N. Advanced data-driven FBG sensor-based pavement monitoring system using multi-sensor data fusion and an unsupervised learning approach. *Measurement* 2025; 242: 115821.
44. Kullback S and Leibler RA. On information and sufficiency. *Ann Math Stat* 1951; 22(1): 79–86.
45. Belov DI and Armstrong RD. Distributions of the Kullback–Leibler divergence with applications. *Br J Math Stat Psychol* 2011; 64(2): 291–309.
46. Hernando D, Tavalaei SAG, Hasheminejad N, et al. Exploring the use of fiber Bragg grating sensors for monitoring the structural response of asphalt pavements. In: Nikolaides AF, Manthos E (eds) *Bituminous mixtures and pavements VIII*. London: CRC Press, 2024, pp. 708–716.